Analysis of multiple scattering suppression using structured laser illumination planar imaging in scattering and fluorescing media

Kristensson, Elias; Araneo, L.; Berrocal, Edouard; Manin, J.; Richter, Mattias; Aldén, Marcus; Linne, M.

Published in:
Optics Express

DOI:
10.1364/OE.19.013647

2011

Analysis of multiple scattering suppression using structured laser illumination planar imaging in scattering and fluorescing media

E. Kristensson,[1,*] L. Araneo,[2] E. Berrocal,[1] J. Manin,[3] M. Richter,[1] M. Aldén,[1] and M. Linne[4]

[1]*Division of Combustion Physics, Lund Institute of Technology Box 118, S-221 00 Lund University, Sweden*
[2]*Politecnico di Milano, Dipartimento di Energia via La Masa 34, 20156 Milano, Italy*
[3]*Universidad Politécnica de Valencia, CMT-Motores Térmicos camino de Vera S/N, 46022 Valencia, Spain*
[4]*Division of Combustion, Chalmers University of Technology, 41296 Gothenburg, Sweden*
[*]*elias.kristensson@forbrf.lth.se*

Abstract: The accuracy, precision and limitations of the imaging technique named Structured Laser Illumination Planar Imaging (SLIPI) have been investigated. SLIPI, which allows multiply scattered light to be diminished, has previously demonstrated improvements in image quality and contrast for spray imaging. In the current study the method is applied to a controlled confined environment consisting of a mixture of water and monodisperse polystyrene microspheres. Elastic scattering and fluorescence are studied and the results obtained when probing different particle concentrations and diameters conclusively show the advantages of SLIPI for imaging within moderately turbid media. Although the technique presents both good repeatability and agreement with the Beer-Lambert law, discrepancies in its performance were, however, discovered. Photons undergoing scattering without changing their incident trajectory cannot be discriminated and, owing to differences in scattering phase functions, probing larger particles reduces the suppression of multiply scattered light. However, in terms of visibility such behavior is beneficial as it allows denser media to be probed. It is further demonstrated that the suppression of diffuse light performs equally well regardless of whether photons propagate along the incident direction or towards the camera. In addition, this filtering process acts independently on the spatial distribution of the multiply scattered light but is limited by the finite dynamic range and unavoidable signal noise of the camera.

OCIS codes: (290.4210) Multiple scattering; (290.7050) Turbid media; (110.0113) Imaging through turbid media; (290.2200) Extinction.

References and links

1. M. A. A. Neil, R. Juškaitis, and T. Wilson, "Method of obtaining optical sectioning by using structured light in a conventional microscope," Opt. Lett. **22**, 1905–1907 (1997).

#145072 - $15.00 USD Received 30 Mar 2011; revised 12 May 2011; accepted 12 May 2011; published 30 Jun 2011

2. L. Krzewina and M. Kim, "Single exposure optical sectioning by color structured illumination microscopy," Opt. Lett. **31**, 477–479 (2006).
3. M. A. A. Neil, R. Juškaitis, and T. Wilson, "Real time 3D fluorescence microscopy by two beam interference illumination," Opt. Commun. **153**, 1–4 (1998).
4. M. J. Cole, J. Siegel, S. E. D. Webb, R. Jones, K. Dowling, M. J. Dayel, D. Parsons-Karavassilis, P. M. W. French, M. J. Lever, L. O. D. Sucharov, M. A. A. Neil, R. Juškaitis, and T. Wilson, "Time-domain whole-field fluorescence lifetime imaging with optical sectioning," J. Microsc. **203**, 246–257 (2000).
5. M. G. L. Gustafsson, "Surpassing the lateral resolution limit by a factor of two using structured illumination microscopy," J. Microsc. **198**, 82–87 (2000).
6. M. G. L. Gustafsson, "Nonlinear structured-illumination microscopy: wide-field fluorescence imaging with theoretically unlimited resolution," Proc. Natl. Acad. Sci. U.S.A. **102**, 13081–13086 (2005).
7. E. Cortizo, A. M. Yeras, J. Lepore, and M. Garavaglia, "Application of the structured illumination method to study the topography of the sole of the foot during a walk," Opt. Laser Eng. **40**, 117–132 (2003).
8. E. Kristensson, M. Richter, S.-G. Pettersson, M. Aldén, and S. Andersson-Engels, "Spatially resolved, singleended two-dimensional visualization of gas flow phenomena using structured illumination," Appl. Opt. **47**, 3927–3931 (2007).
9. T. Breuninger, K. Greger, and E. H. K. Stelzer, "Lateral modulation boosts image quality in single plane illumination fluorescence microscopy," Opt. Lett. **32**, 1938–1940 (2007).
10. E. Berrocal, E. Kristensson, M. Richter, M. Linne, and M. Aldén, "Application of structured illumination for multiple scattering suppression in planar laser imaging of dense sprays," Opt. Express **16**, 17870-17881 (2008).
11. E. Kristensson, E. Berrocal, M. Richter, S. Pettersson, and M. Aldén, "High-speed structured planar laser illumination for contrast improvement of two-phase flow images," Opt. Lett. **33**, 2752-2754 (2008).
12. M. Jermy and D. Greenhalgh, "Planar dropsizing by elastic and fluorescence scattering in sprays too dense for phase doppler measurement," Appl. Phys. B **71**, 703–710 (2000).
13. E. Kristensson, E. Berrocal, M. Richter, and M. Aldén, "Nanosecond structured laser illumination planar imaging for single-shot imaging of dense sprays," Atomization Spray **20**, 337–343 (2010).
14. P. L. Gal, N. Farrugia, and D. A. Greenhalg, "Laser sheet dropsizing of dense sprays," Opt. Laser Technol. **31**, 75–83 (1999).
15. D. G. Talley, J. F. Verdieck, S. W. Lee, V. G. McDonell, and G. S. Samuelsen, "Accounting for laser sheet extinction in applying PLLIF to sprays," paper AIAA-96-0469, presented at the Thirty-Fourth Aerospace Sciences Meeting, Reno, Nev., 15–18 Jan. 1996 (American Institute of Aeronautics and Astronautics, New York, 1996).
16. M. Linne, M. Paciaroni, E. Berrocal, and D. Sedarsky, "Ballistic imaging of liquid breakup processes in dense sprays," in *Proceedings of the Combustion Institute*, (2009), pp. 2147–2161.
17. J. V. Pastor, R. Payri, L. Araneo, and J. Manin, "Correction method for droplet sizing by laser-induced fluorescence in a controlled test situation," Opt. Eng. **48**, 1–11 (2009).
18. L. Callegaro, F. Pennecchi, and P. G. Spazzini, "Comparison of calibration curves using the L_p norm," Accred. Qual. Assur. **14**, 587–592 (2009).

1. Introduction

Structured illumination is an imaging technique originally introduced for microscopy in 1997 [1]. The main purpose of the method is to remove out-of-focus light that degrades the sectioning capability of line-of-sight optical arrangements. Since then, the technique has been widely applied [2–4], and for much more than its original purpose. Gustafsson illustrated that the technique could be used to surpass the diffraction limit, achieving theoretically unlimited resolution [5, 6]. Although the majority of publications related to structured illumination concern microscopic imaging, the technique has also been applied outside this field. Cortizo et al. used a structured light source to study the topography of the sole of the foot during a walk [7] while Kristensson et. al implemented the technique for the study of a dynamic flow of water droplets [8].

In 2007 it was demonstrated, on a static microscopic biological sample, how the method could be combined with a planar illumination scheme [9]. This approach proved advantageous for macroscopic imaging of turbid media, such as atomizing spray systems [10, 11]. When probing such media, multiply scattered light (also referred to as *diffuse light*) degrades the resulting images e.g. via blurring and is considered as the major source of error for measurements within dense media [12]. Implementing structured illumination allows this unwanted intensity contribution to be diminished. As this light contains little or no structural information from

#145072 - $15.00 USD Received 30 Mar 2011; revised 12 May 2011; accepted 12 May 2011; published 30 Jun 2011

the illuminated section, such suppression increases the image contrast and it visualizes sample structures which may be normally concealed by blurring [13]. This planar imaging approach named Structured Laser Illumination Planar Imaging (SLIPI) is, however, not restricted to qualitative measurements. Because of its noise filtering capabilities, SLIPI has potential to improve both the accuracy and precision of currently existing laser sheet techniques (that are based on single scattering detection) when applied in relatively dense scattering media. This could involve droplet sizing using Planar Droplet Sizing [14] or determination of liquid volume fraction using Planar Laser Induced Fluorescence [15] for example. Before combining SLIPI with such techniques, the fundamental principles governing the filtering of the diffuse light must be fully understood, which is the aim of the current study.

The main concept with SLIPI is that when photons are multiply scattered, they lose the structural image information contained in the laser sheet and can therefore be suppressed in the image post-processing. This implies, however, that if photons have been scattered without changing the incident trajectory prior to detection they cannot be suppressed despite being multiply scattered. As the probability for this to occur is governed by the scattering phase function, which for Mie scattering is strongly size dependent, SLIPI is expected to suppress a smaller amount of multiply scattered light when larger particles are probed due to an increased preferential forward scattering. This can be considered as a reduced *accuracy* of the technique. Another uncertainty is whether the suppression process depends on the magnitude of the multiply scattered light being detected, which can be considered as the *precision* of SLIPI. High precision is crucial for quantitative measurements as the amount of multiply scattered light cannot be predetermined. Finally, unlike other advanced imaging techniques that also are capable of diminishing multiply scattered light, e.g. Ballistic imaging [16], SLIPI does not inhibit the *detection* of such light. The suppression is instead performed in the image post-processing, making SLIPI restricted to less turbid media (up to an optical depth of ~ 6). When probing a sample with too high turbidity almost all detected light has been multiply scattered and extracting the weak contribution of singly scattered light leads to a noisy and unreliable SLIPI image. However, at present this upper turbidity limit for SLIPI is unknown.

For these reasons, the current study aims to quantify the capabilities and limitations of the SLIPI technique for both elastic scattering and fluorescence. To achieve this end, independent knowledge of the sample characteristics is required. A controlled environment consisting of a homogeneous mixture of monodisperse polystyrene spheres, doped with dye, and water was therefore chosen, similar to [17], as this allows the SLIPI results to be compared with the Beer-Lambert relation.

2. Structured laser illumination planar imaging

The fundamental principle of SLIPI is to combine structured illumination and planar laser imaging, practically achieved by superimposing a Ronchi grating on a laser sheet for example. This creates a line pattern that serves as a signature when it illuminates the interior of a scattering medium and is used to distinguish between singly scattered and diffuse light. In contrast to singly scattered photons, multiply scattered photons lose the incident signature and will appear as intensity noise (whose magnitude depends on the optical characteristics of the sample). Thus, the local undisturbed amplitude of the modulation becomes a measure of the amount of directly scattered light. To extract this information, the amplitude is converted into intensity. Experimentally, this involves the recording of a minimum of three intensity modulated images, between which the line structure is physically shifted vertically. Equation (1) describes the resulting image $I(x,y)$ when a sample is illuminated with a sinusoidal intensity modulation.

$$I(x,y) = I_C(x,y) + I_S(x,y) \cdot \cos(2\pi\nu y + \phi), \tag{1}$$

#145072 - $15.00 USD Received 30 Mar 2011; revised 12 May 2011; accepted 12 May 2011; published 30 Jun 2011

where ν denotes the modulation frequency, ϕ the spatial phase, and $I_C(x,y)$ and $I_S(x,y)$ the local intensity offset and amplitude, respectively. Ideally, when no diffuse light is detected the illuminated sample is described by either I_C or I_S. By moving the line structure vertically, i.e. changing ϕ, the directly scattered light is shifted accordingly. However, light that does not represent the intensity modulation remains unaffected. This light contribution arises from photons that have experienced several scattering events prior to detection. Therefore, by studying the absolute difference between the modulated images, according to Eq. (2), all similar intensity features (multiply scattered light) are diminished while all unique image features, arising primarily from directly scattered light, are kept.

$$SLIPI = I_S = \frac{\sqrt{2}}{3}\sqrt{(I_1 - I_2)^2 + (I_1 - I_3)^2 + (I_2 - I_3)^2} \tag{2}$$

Equation (2) shows how a SLIPI image is extracted from three phase shifted images, between which the spatial phase (ϕ) is shifted 120 degrees. Furthermore, the technique allows the *conventional image* to be reconstructed by taking the average of the raw data images, as shown in Eq. (3). This image is, theoretically, equal to that acquired when employing a non-modulated homogeneous laser sheet, allowing the results from the two techniques to be compared.

$$Conv = I_C = \frac{1}{3}\sum_{i=1}^{3} I_i \tag{3}$$

since

$$\sum_{i=1}^{3} I_i = 3 \cdot I_C + I_S \cdot \underbrace{(cos(2\pi\nu y + 0) + cos(2\pi\nu y + 120) + cos(2\pi\nu y + 240))}_{=0} \tag{4}$$

A graphical explanation of Eqs. (1)–(3) is illustrated in Fig. 1. Here, a signal I_C is recorded with an unknown intensity offset, Fig. 1 (a). This offset represents the total light contribution of multiple scattering. Notice how the implementation of thresholding (to remove the diffuse light) on the recorded signal would induce errors as the offset varies throughout the entire signal. In Fig. 1(b), the sample is instead probed using a modulated intensity (Eq. (1)). Assuming laser extinction and signal attenuation effects to be absent, the local amplitude provides information that truly represents the probed sample. This can be seen in Fig. 1(c), that shows the product $I_S(x,y) \cdot \cos(2\pi\nu y + \phi)$. Implementing Eq. (2) converts the envelope of the modulation into signal intensity which is directly related to the scattering property of the probed sample, Fig. 1(d).

3. Experimental arrangement

An intensity modulated laser sheet was created by imaging a Ronchi grating (10 line pairs/mm) onto the sample while simultaneously optically compressing the beam in the depth direction, thus creating sheet of light (thickness $\sim$100 μm) with a slight vertical divergence. Higher order interference frequencies generated from a square Ronchi pattern were removed by an aperture (frequency cutter). To acquire a near top-hat intensity profile only the central part of the quasi gaussian beam was selected. Phase shifting was achieved by tilting a glass plate situated directly after the Ronchi grating. To account for even minimal laser fluctuations, the incident profile was monitored and used as a normalization factor in image post-processing.

The measurement volume consisted of a glass cell (44 $\times$ 34 $\times$ 100 mm^3, Hellma large cell, cat. number 740.000-OG) containing a dispersion of monodisperse scattering and fluorescing particles (volumetrically doped with dye, Duke Scientific Fluorescent Polymer Dry

#145072 - $15.00 USD Received 30 Mar 2011; revised 12 May 2011; accepted 12 May 2011; published 30 Jun 2011

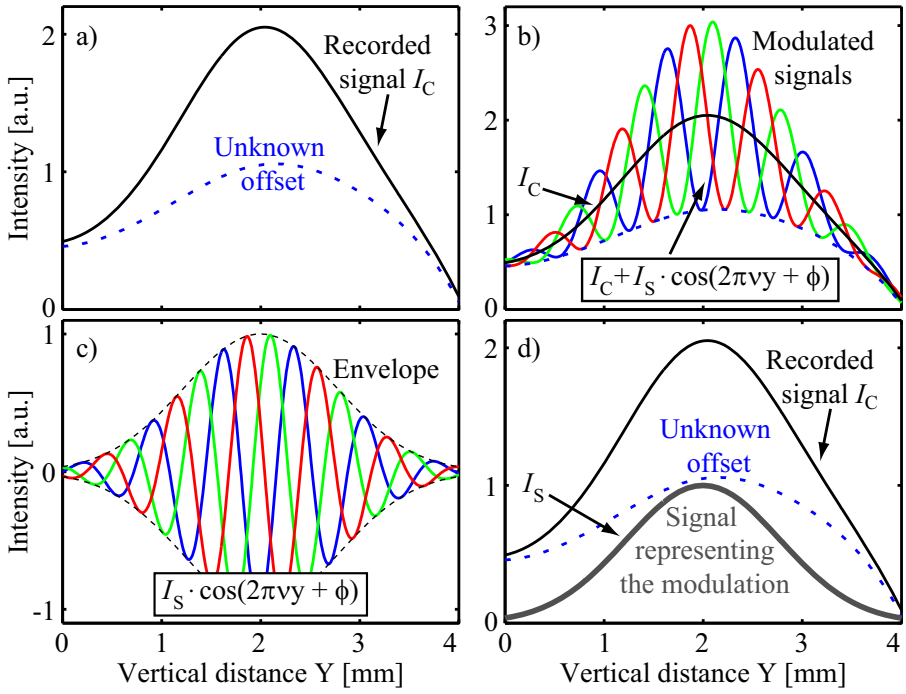

Fig. 1. Graphical example of Eqs. (1)–(3). (a) The recorded signal with an unknown intensity offset. (b) A modulated illumination scheme is applied. (c) The local amplitude of the modulation. (d) Equation (2) is applied, converting the envelope in (c) into intensity. As the unwanted offset is identical in all three recordings it is removed through Eq. (2).

Microspheres) mixed with distilled water. To achieve an average homogeneous concentration, the mixture was continuously stirred using a magnetic stirrer and prior to each experiment session possible particles aggregates were separated by ultrasonic treatment. Three particle sizes were studied and for each solution three different optical depths (*OD*) were investigated. The different concentrations were obtained by first calculating the extinction cross section, based on the Mie theory. This was then used to calculate the number of particles required for the various optical depths and finally, each mixture was prepared by weighing the particles.

Furthermore, by translating the cell different sections within the cell could be probed (see Fig. 2). Image focus was maintained by simultaneously shifting the camera position to compensate for the different thicknesses of water in front of the laser sheet. The sections studied here will be referred to as S_2, S_{12}, S_{22} and S_{32}, corresponding to a depth of 2, 12, 22 and 32 mm into the cuvette, respectively, along the 34 mm cell thickness.

The illumination source consisted of a frequency doubled pulsed Nd:YAG laser, emitting radiation at 532 nm. The elastically scattered light and the laser induced fluorescence, with an emission peak around 612 nm, were spectrally separated using either a band-pass or a long-pass filter, respectively. A 14-bit Andor iXon camera (DV-887) with a resolution of 512 $\times$ 512 pixels was used to record the images. Figure 2 shows a schematic of the optical arrangement together with an example of a recorded image. All experiments were conducted for both elastic (Mie) scattering and fluorescence (LIF) and for each individual case a total of 1500 images were recorded. The resulting 72 different measurement cases are summarized in Table 1.

During the experiments, great care was taken to avoid saturation of the dye. This is of utmost importance as this would cause the fluorescence signal to deviate from the Beer-Lambert

#145072 - $15.00 USD Received 30 Mar 2011; revised 12 May 2011; accepted 12 May 2011; published 30 Jun 2011

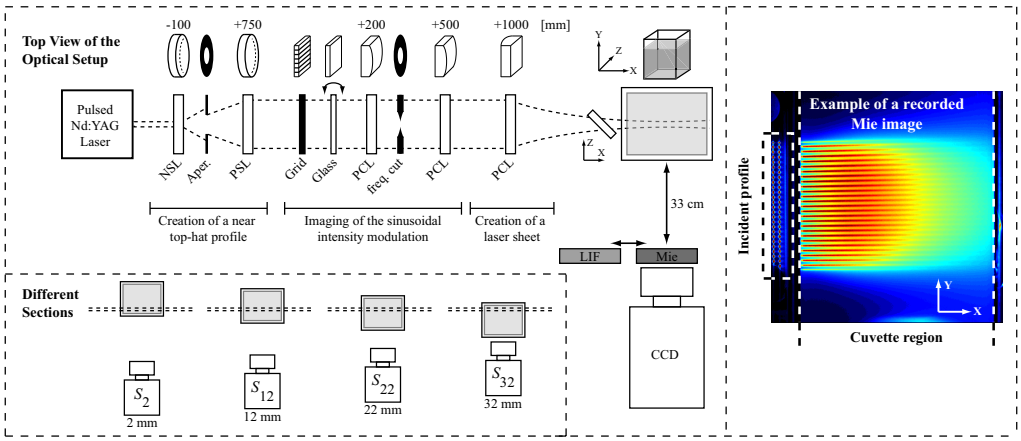

Fig. 2. Schematic of the optical arrangement for the SLIPI setup together with an example of a recorded image. Also provided is an illustration of the four different sections within the measurement volume. NSL = Negative Spherical Lens, Aper. = Aperture, PSL = Positive Spherical Lens, PCL = Positive Cylindrical Lens and freq. cut = Frequency Cutter. Note that the imaging part of the setup is the only difference between that of an ordinary laser sheet arrangement and SLIPI.

Table 1. Summary of the Different Measurements Performed*

Diameter [μm]	*OD*	Section [mm]	Scattering Process
7, 15 and 31	2, 4 and 6	2, 12, 22 and 32	Mie and LIF

*For each particle size all combinations of *OD*, scattering processes and sections within the cell were probed. From each case, both the SLIPI and conventional images were extracted.

relation, which is the basis for the analysis of the results. To investigate whether saturation occurred the incident light intensity was steadily increased to study eventual changes in the detected modulation. As demonstrated by Gustafsson [6], saturation causes the incident sinusoidal modulation pattern to be distorted which leads to the presence of higher order harmonics. By the use of Fourier analysis and by comparing elastic scattering (which does not suffer from such a distortion) with fluorescence it could be concluded that no saturation of the dye occurred with the laser power used throughout the experiments.

4. Experimental results

Figure 3 shows the resulting conventional and SLIPI images (all normalized to unity) for both Mie scattering and fluorescence, acquired at S_{12} (see Fig. 2). To interpret and analyze these results, a vertical summation over the laser sheet area for each recording is extracted. Figure 4 shows the resulting intensity curves for both Mie scattering and fluorescence obtained using conventional planar laser imaging. Here, each graph contains the four measurements performed at the different sections within the cuvette (from S_2 to S_{32}) for a given optical depth and particle size. No comparison in detected intensity between the Mie and LIF signals will be made and therefore the curves for the different scattering processes are normalized to unity with respect to the highest detected value at distance x = 0 mm. In the Mie case, this corresponds to the measurement performed on 7 μm at S_2 and *OD* 6. For fluorescence, the corresponding measurement case was for 31 μm at S_2 and *OD* 6.

As light travels through a turbid medium its un-scattered intensity decays exponentially with

#145072 - $15.00 USD Received 30 Mar 2011; revised 12 May 2011; accepted 12 May 2011; published 30 Jun 2011

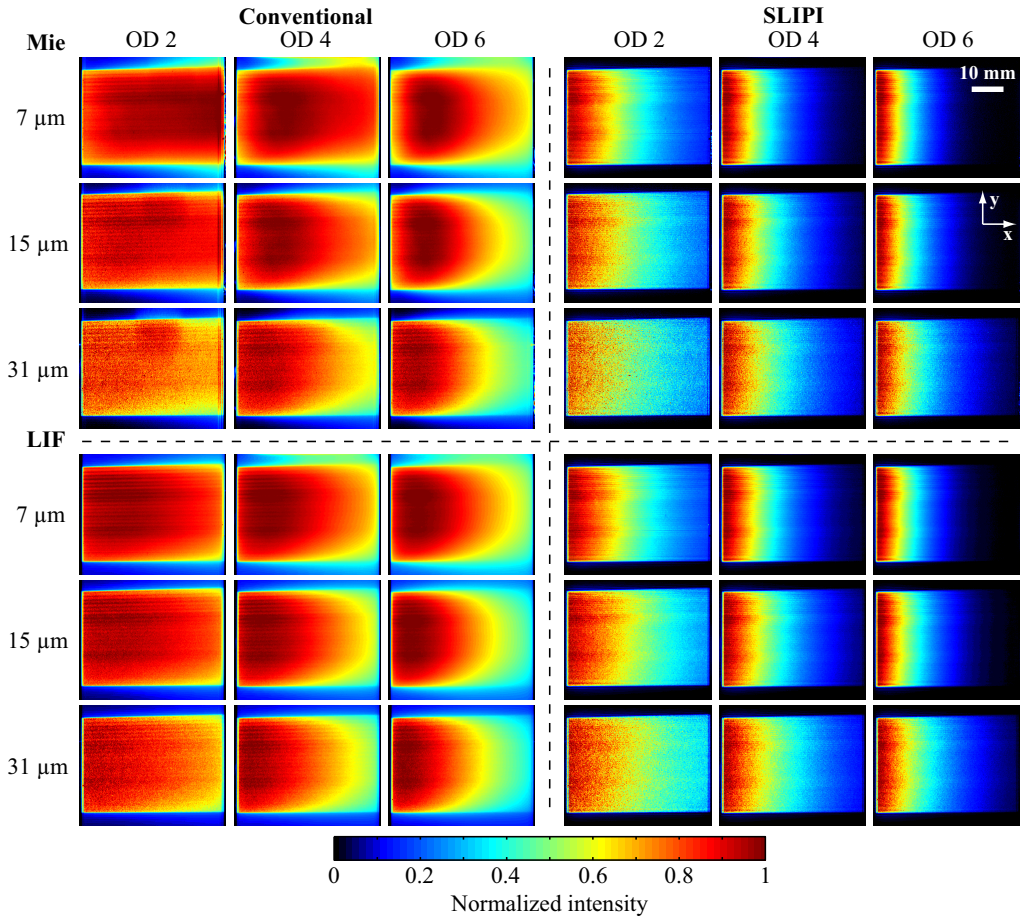

Fig. 3. (*Left*): Conventional planar laser imaging. (*Right*): SLIPI. The images were recorded at S_{12}.

distance according to the Beer-Lambert law. This behavior is, however, not seen in the intensity curves in Fig. 4 because both singly and multiply scattered light is detected. The peculiar shape of these curves illustrates the complexity of multiple scattering as it is seen that its contribution varies for each individual measurement case.

Vertical summations are also extracted from the SLIPI data and they are presented in Fig. 5 together with the intensity decay predicted by the Beer-Lambert law (dashed line). To illustrate the repeatability and precision of the technique, all curves are normalized to unity. However, the number given in the upper right corner indicates the relative intensities at $x = 0$ mm for each curve.

#145072 - $15.00 USD Received 30 Mar 2011; revised 12 May 2011; accepted 12 May 2011; published 30 Jun 2011

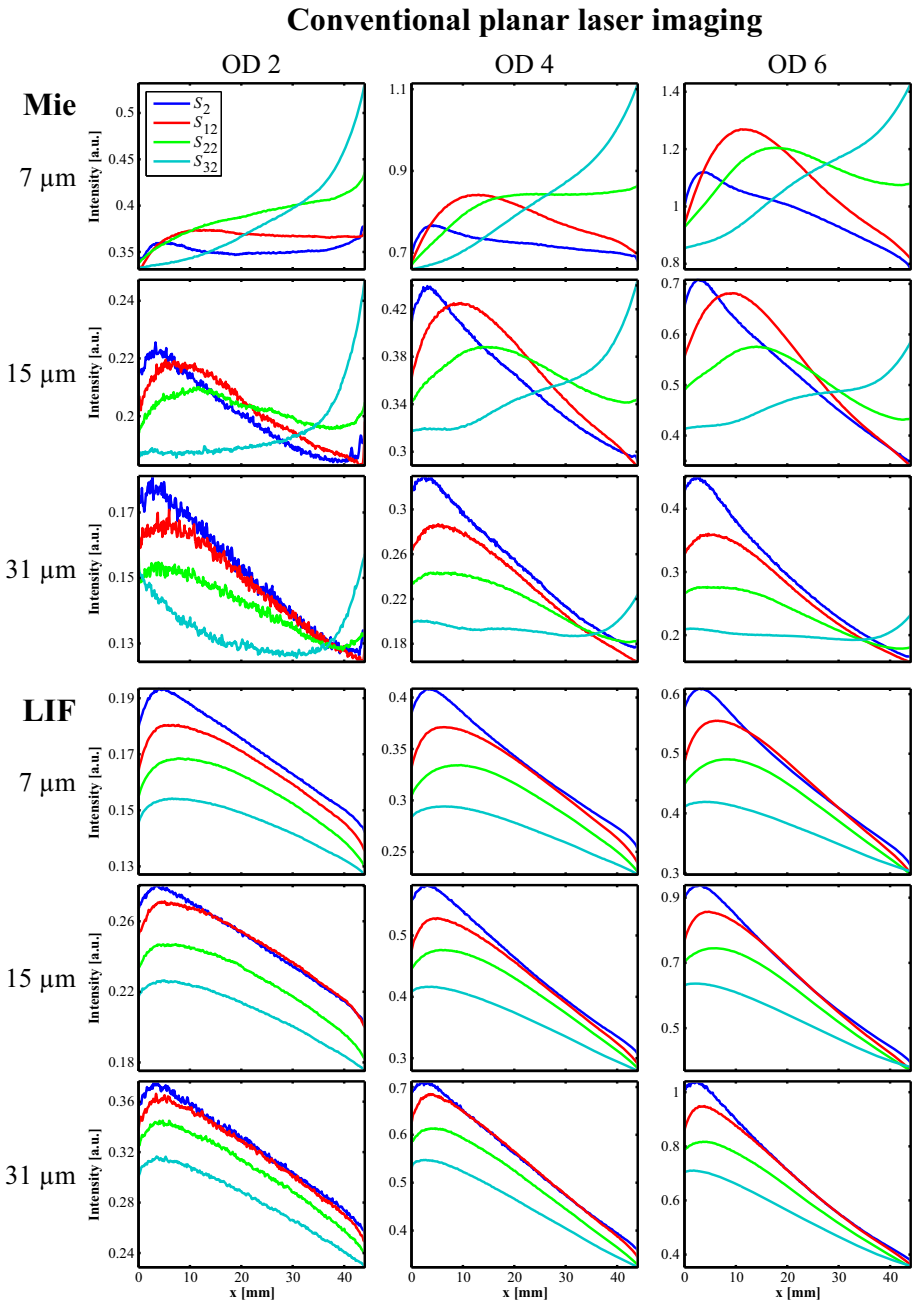

Fig. 4. Vertical summation of the result obtained using conventional planar imaging for both Mie scattering and fluorescence. All results are normalized with respect to the highest detected value at $x = 0$ mm for the corresponding scattering process.

#145072 - $15.00 USD Received 30 Mar 2011; revised 12 May 2011; accepted 12 May 2011; published 30 Jun 2011

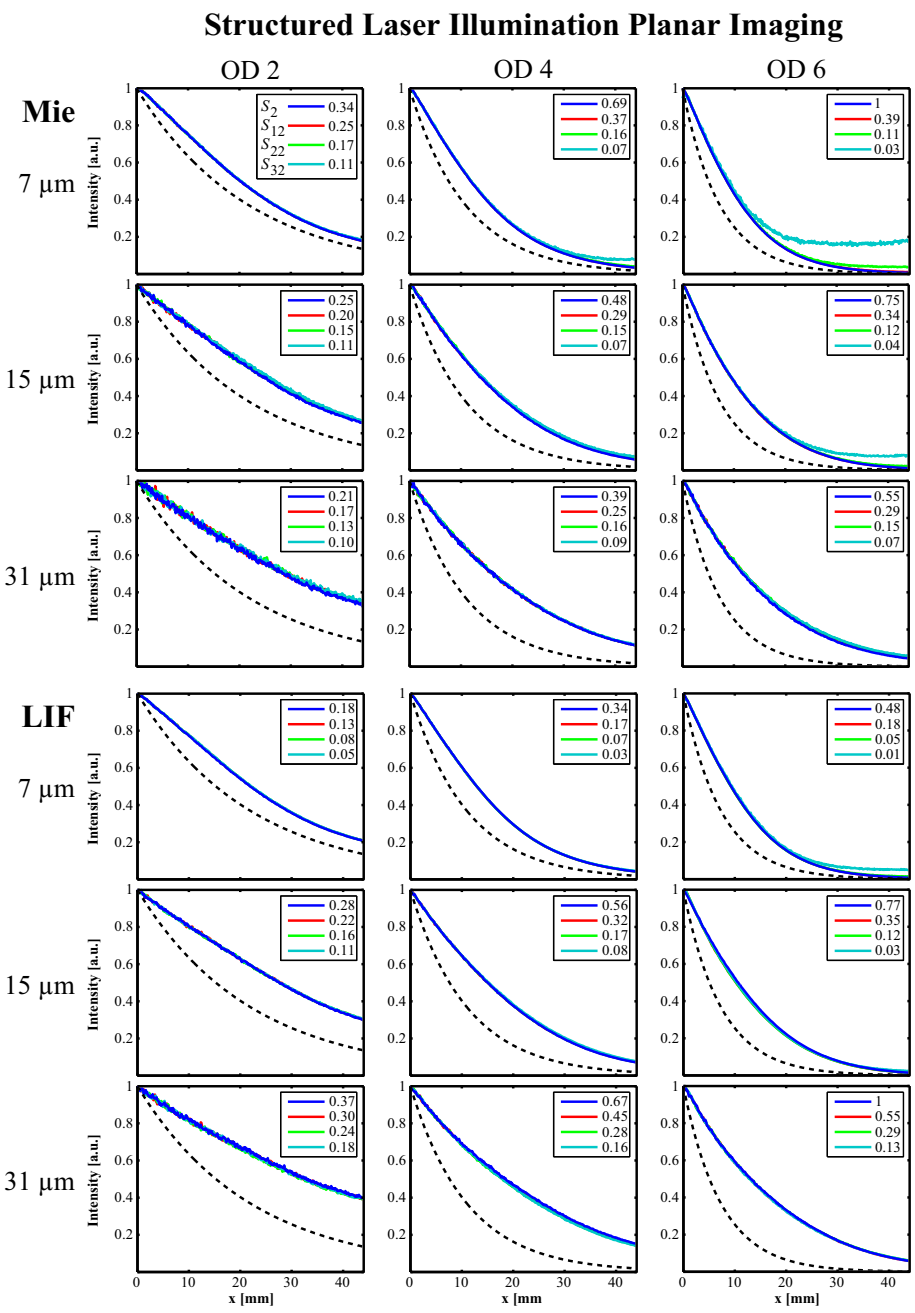

Fig. 5. Vertical summations of the results obtained using SLIPI for both Mie scattering and laser induced fluorescence. All results are normalized to unity to illustrate the precision of the technique. The normalization factor (detected intensity at $x = 0$ mm) is reported in the legend. The dashed line shows the Beer-Lambert decay.

#145072 - $15.00 USD Received 30 Mar 2011; revised 12 May 2011; accepted 12 May 2011; published 30 Jun 2011

5. Analysis

In this section the analysis of the results for both conventional planar laser imaging and SLIPI is presented. The accuracy and precision for both techniques are estimated from the intensity curves in Fig. 4 and 5. Note that apart from multiple scattering issues, the detected light suffers from both signal attenuation and laser extinction. However, because of the homogeneity of the sample these two phenomena can be treated separately, which reduces the complexity of the analysis.

5.1. Calculation of accuracy and precision

Illuminating a homogeneous sample with known optical characteristics provides independent knowledge, helping to interpret the results. First, one would expect the incident light intensity to decay exponentially with distance, due to laser extinction. The rate at which the intensity decays is related to the number density of particles and can be derived from the Beer-Lambert law, described in Eq. (5).

$$I(x,y) = I_0(y) \cdot e^{-N \cdot \sigma_e \cdot x} = I_0(y) \cdot e^{-\mu_e \cdot x} \tag{5}$$

Here the sample is assumed to be homogeneous with an extinction coefficient μ_e and a number density of N particles that have an extinction cross-section σ_e. After a scattering or absorption event has occurred, the photon energy is assumed to be lost. Therefore, if multiply scattered light is detected the results will deviate from the Beer-Lambert law. One straightforward approach to determine the diffuse light filtering capabilities is thus to compare the SLIPI results with this relation. Deviation from this *a priori* decay of light intensity is an indication that multiply scattered light is still present in the final SLIPI image. Quantifying this deviation provides a measure of the *accuracy* of SLIPI. A high accuracy should be interpreted as though near all multiply scattered light is suppressed and that the result follows the Beer-Lambert law.

In addition, probing sections deeper into the cuvette with SLIPI should result in an overall reduced signal due to signal attenuation. However, owing to the homogeneity of the sample, the decay along the x-axis should, theoretically, be identical. By normalizing these decays and comparing each measurement case allows the *precision* of SLIPI to be investigated, where the precision quantifies how well the decays (for the different sections) overlap spatially. This is of interest as the contribution of multiply scattered light is likely to vary between the different sections. Thus, a high precision implies that SLIPI is able to accurately extract the same signal, regardless of the accompanied noise level. Based on these parameters - accuracy and precision - the capabilities and limitations of SLIPI can be evaluated for different particle sizes as well as for different magnitudes of turbidity.

To determine how well the curves obtained at the four different sections spatially overlap, i.e. the precision, S_2 is compared with S_{12}, S_{22} and S_{32} using the Least Power norm L_p with p = 1 according to Eq. (6) (terminology adopted from [18]). By integrating the absolute difference between the curves a quantification of the overlap is performed. A low value of p gives a measure of the overall similarity of the curves, which is the reason for choosing p = 1. Higher values could also be used but highlights instead the maximum local differences [18].

$$L_p = \left(\frac{1}{44} \cdot \int_0^{44} |I_{ref}(x) - I(x)|^p dx \right)^{1/p} \tag{6}$$

where the value 44 refers to the total x-distance in millimeters, I_{ref} corresponds to the measurement performed at S_2 (which is the least affected by signal attenuation and multiple scattering), while the remaining sections (S_{12} to S_{32}) are described by I. Both I_{ref} and I are normalized to

#145072 - $15.00 USD Received 30 Mar 2011; revised 12 May 2011; accepted 12 May 2011; published 30 Jun 2011

unity at x = 0 mm. Thus, a good spatial overlap will result in an L_p close to zero while the opposite case gives an increased value. Even though there is no actual upper limit for L_p, the values are expected to be within the range $0 \leq L_p \leq 1$. This is because the intensity is normalized at x = 0 mm after which it is expected to decrease (L_p can only be larger than 1 if the intensity at a given section instead increases significantly with distance, compared to I_{ref}). Therefore, to present the precision in a more representative fashion the L_p values are used to express the precision using the following equation.

$$P = 100 * (1 - L_p) \tag{7}$$

With this approach P = 100 indicates that I_{ref} and I coincide everywhere. Table 2 shows a complete summary of the calculated values for precision. For comparison reasons only, the estimated precision for conventional imaging is also presented here.

Table 2. Calculations of the P Term*

	Structured Laser Illumination Planar Imaging								
Size	7 μm			15 μm			31 μm		
Section	S_2-S_{12}	S_2-S_{22}	S_2-S_{32}	S_2-S_{12}	S_2-S_{22}	S_2-S_{32}	S_2-S_{12}	S_2-S_{22}	S_2-S_{32}
	Mie scattering								
OD = 2	100	100	100	99	100	100	99	99	99
OD = 4	100	100	99	99	99	100	98	99	99
OD = 6	100	99	92	99	99	98	98	99	99
	Laser Induced Fluorescence								
OD = 2	100	100	100	100	100	99	99	99	100
OD = 4	100	100	100	100	100	99	99	99	100
OD = 6	100	100	98	100	99	99	99	99	99
	Conventional planar laser imaging								
	Mie scattering								
OD = 2	93	89	86	94	86	83	96	90	87
OD = 4	88	81	76	89	80	74	94	86	80
OD = 6	82	75	67	88	75	64	93	80	71
	Laser Induced Fluorescence								
OD = 2	95	90	88	95	91	91	97	94	91
OD = 4	95	89	87	96	90	90	97	94	91
OD = 6	95	91	90	97	92	91	98	95	92

*The results are acquired using Eq. (7).

To estimate accuracy the same approach is used, i.e. with the Least Power norm (p = 1). However, these calculations aim at quantifying how close to the Beer-Lambert decay the results are. For this reason, I_{ref} is instead set by Eq. (5), where μ_e is determined by the different optical depths, while I represents the decays (normalized to unity at x = 0 mm) presented in either Fig. 4 or 5. A value of P close to 100 thus indicates low divergence from the Beer-Lambert decay. As mentioned previously, L_p has no upper boundary and thereby a negative value of P is possible. This occurs, however, only when the detected light intensity increases at a higher rate than what the intensity according to the Beer-Lambert law is decreasing (see e.g. the Mie intensity curve at S_{22} for 7 μm and $OD = 6$ in Fig. 4). A negative value of P is thus indicating that the amount of multiply scattered light greatly exceeds the directly scattered. Note also that due to the normalization of I the absolute intensity level is not taken into account, which could lead to an overestimation of the accuracy for both imaging techniques.

#145072 - $15.00 USD Received 30 Mar 2011; revised 12 May 2011; accepted 12 May 2011; published 30 Jun 2011

Table 3. Estimations of the Accuracy for Both SLIPI and Conventional Imaging*

Structured Laser Illumination Planar Imaging												
Size	7 μm				15 μm				31 μm			
Section	S_2	S_{12}	S_{22}	S_{32}	S_2	S_{12}	S_{22}	S_{32}	S_2	S_{12}	S_{22}	S_{32}
	Mie scattering											
OD = 2	90	90	90	90	85	85	85	84	80	79	79	79
OD = 4	90	90	90	89	86	86	86	85	81	81	81	80
OD = 6	91	91	90	83	89	89	89	87	83	82	82	82
	Laser Induced Fluorescence											
OD = 2	88	87	87	87	82	82	82	82	76	77	77	77
OD = 4	88	88	88	88	84	83	83	83	77	78	78	78
OD = 6	90	90	90	88	86	87	87	87	80	80	80	80
Conventional planar laser imaging												
	Mie scattering											
OD = 2	37	30	26	25	49	44	39	38	54	49	48	52
OD = 4	19	7	1	-2	35	21	15	12	46	36	31	26
OD = 6	18	0	-6	-13	36	19	10	1	48	35	28	19
	Laser Induced Fluorescence											
OD = 2	46	41	40	41	50	45	46	47	52	49	49	50
OD = 4	36	26	24	27	42	33	32	35	45	39	39	40
OD = 6	34	22	22	25	41	32	31	33	47	38	38	39

*The calculations are based on Eq. (6) and (7). I_{ref} is set by the Beer-Lambert decay.

The results presented in Table 3 indicate how close to the theoretical exponential decay the results are along the incident direction. However, they do not provide information regarding the reduction of intensity for light traveling towards the camera, i.e. signal attenuation (also described by the Beer-Lambert relation). To investigate this the Least Power norm (Eq. (6)) can once again be implemented. This will show whether the suppression of multiple scattering acts differently as photons travel either towards the camera or along the incident direction. Table 4 shows the corresponding values of P, calculated using Eqs. (6) and (7) where I_{ref} is set by the Beer-Lambert decay while I is constructed from the intensity values at x = 0 mm for S_2 to S_{32}.

Table 4. Estimated Accuracy for Both SLIPI and Conventional Imaging for the Reduction of Light Intensity as Photons Propagate towards the Camera*

SLIPI / Conventional imaging						
Size	7 μm	15 μm	31 μm	7 μm	15 μm	31 μm
	Mie			LIF		
OD = 2	90 / 42	81 / 52	77 / 49	92 / 55	83 / 55	77 / 53
OD = 4	91 / 23	84 / 37	78 / 47	92 / 40	86 / 40	77 / 37
OD = 6	92 / 20	88 / 36	80 / 49	93 / 32	89 / 32	79 / 33

*Values to the left or right hand side of the division sign show the results for either SLIPI or conventional imaging, respectively.

5.2. Analysis of accuracy and precision

The results in Tables 2–4 together with observations that can be made on the results presented in Fig. 3–5 clearly demonstrate the complex nature of multiple scattering. Its contribution depends on the particle size, scattering process involved as well as the media surrounding the laser sheet

#145072 - $15.00 USD Received 30 Mar 2011; revised 12 May 2011; accepted 12 May 2011; published 30 Jun 2011

which makes correction approaches extremely challenging. For the measurements presented in this study the amount of multiply scattered light is additionally influenced by the confinement of the sample. Photons reflected on the windows that should not have been detected are redirected towards the camera. This is seen as an increase of intensity near the exit side of the cuvette in the Mie measurements in Fig. 4. This is avoided to some extent by optically filtering out the elastically scattered light, which is seen in Tables 2–4 where the LIF measurements with conventional imaging give rise to both higher precision and accuracy in general.

Qualitative improvements in image quality when applying SLIPI can be seen in Fig. 3. In contrast to conventional imaging, the near top-hat laser sheet profile becomes visible with decreasing intensity with distance. These images also possess sharp gradients between illuminated parts of the sample and the surroundings. The precision of SLIPI can be qualitatively visualized in Fig. 5. The close overlap of the different curves and the values presented in Table 2 conclusively illustrates the precision and repeatability of SLIPI. As seen in the conventional results, the contribution of multiply scattered light is strongly influenced by the position (section) of the laser sheet. It can therefore be concluded that the filtering capabilities of SLIPI are independent of the spatial distribution of the diffuse light being detected.

The shape of the intensity reduction, also seen in Fig. 5, tends promisingly towards the Beer-Lambert decay, also illustrated quantitatively in Table 3. Being able to acquire results that follow a known physical relation is key in order to perform quantitative measurements. The results presented in Tables 2–4 thus show that the implementation of SLIPI will improve the quality of such measurements for relatively dense samples (for an optical depth up to ~ 6).

However, in Table 2–4, as well as in Fig. 5, some distinct discrepancies in the SLIPI results are noticed. For conventional imaging, measurements performed on smaller particles give rise to less accurate results. This should be interpreted as though a relatively larger amount multiply scattered light is detected (with respect to the singly scattered), which increases the divergence from the Beer-Lambert decay. In contrast, the accuracy of SLIPI appears to be oppositely related to size. For 7 μm, the average accuracy (from Table 3) for Mie measurements performed on *OD* 2 using SLIPI is 90. When probing 15 μm, this value is reduced to 85 and further decreased for 31 μm to 79. For fluorescence the corresponding values are 87, 82 and 77, respectively. Figure 6 illustrates this effect, where the SLIPI results are shown in a natural logarithmic scale. The upper graphs, denoted “Laser Extinction”, show how the light intensity is reduced along the incident direction while the signal reduction for light traveling towards the camera is provided in the lower graphs, labeled “Signal Attenuation”. Note the different x axes used here (one for each level of turbidity), which enables the measurement performed at different optical depths to be compared with each other.

The curves presented in Fig. 6 clearly illustrate how the filtering process of SLIPI acts differently depending on the particle size being probed. This effect arises from differences in the scattering phase functions. Smaller particles have a less pronounced forward scattering lobe and therefore a scattering event is more likely to result in a change in photon trajectory when probing 7 μm, compared to 31 μm. This explains the peculiar shapes (and reduced accuracy) of the intensity curves for 7 μm in the conventional cases presented in Fig. 4, where a larger amount of multiply scattered light is directed towards the camera. These fundamental differences in light-matter interaction, explained by the Mie theory, greatly influence the appearance of the multiply scattered light contribution. This can be illustrated visually by illuminating the homogeneous sample with a structured laser sheet, as exemplified in Fig. 7 where three cells are probed, all equally turbid (*OD* 6). In this figure it is demonstrated how the line structure remains visible further into the medium when probing 31 μm. The local amplitude of the modulation, which through Eq. (2) is converted into intensity, is therefore less reduced with distance. This phenomenon is due to forward scattering events and gives a false indication of the un-

#145072 - $15.00 USD Received 30 Mar 2011; revised 12 May 2011; accepted 12 May 2011; published 30 Jun 2011

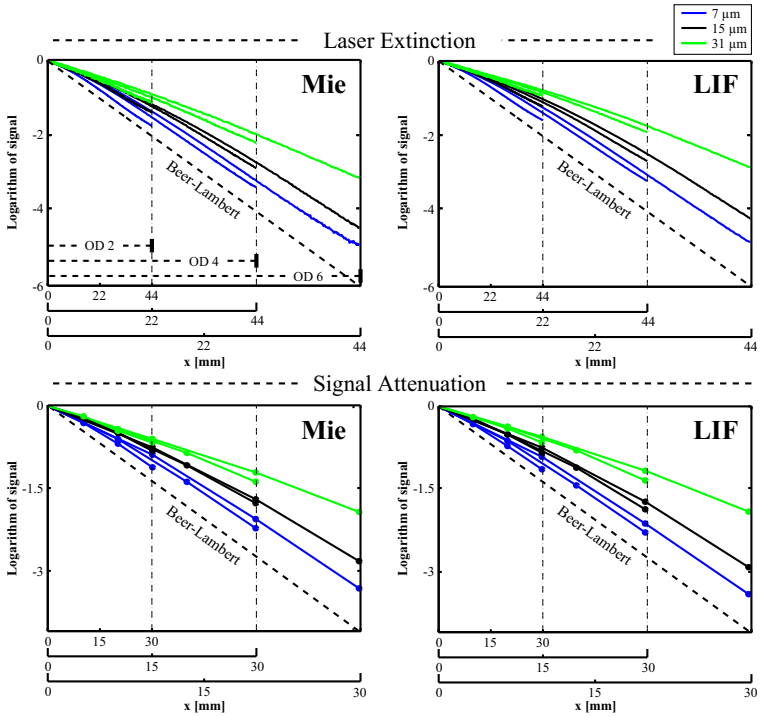

Fig. 6. Deviations in the performance of SLIPI when probing different particle sizes. (*Upper graphs:*) The response when light is traveling along the incident direction of the illumination (at section S_2). (*Lower graphs:*) The reduction of intensity for light propagating towards the camera. Note the natural logarithmic scale on the *y*-axis and the three different *x*-axes (one for each optical depth).

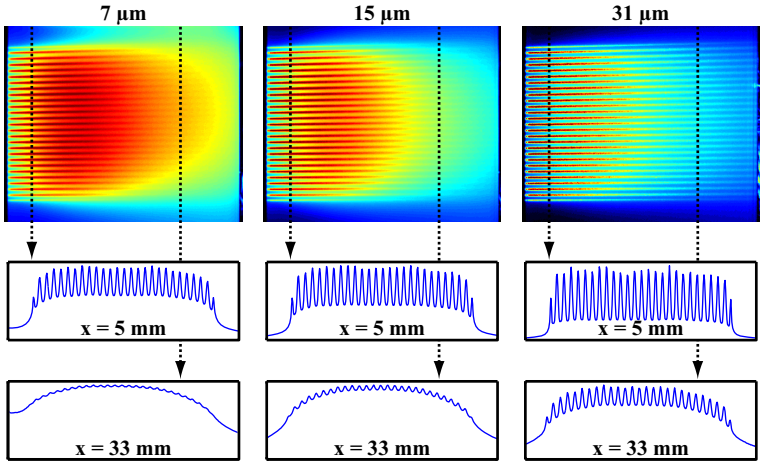

Fig. 7. Examples of Mie scattering from a structured laser sheet for the three different sizes at *OD* 6. Notice how the modulated light remains visible further into the sample when larger particles are probed. Consequently, the amplitude, which is given below each image at two *x* locations, is less reduced with distance for 31 μm.

#145072 - $15.00 USD Received 30 Mar 2011; revised 12 May 2011; accepted 12 May 2011; published 30 Jun 2011

scattered penetration length of light into the sample. SLIPI, which is based on removing light that deviates from the incident trajectory, cannot differentiate between this multiple scattering contribution and the directly scattered light. This fundamental limitation of SLIPI is difficult (if possible) to corrected for as it may require the size distribution of the probed sample to be known. Therefore, the best approach to reduce the effect is to improve the effectiveness of the diffuse light filtering by e.g. increasing the line frequency. This could increase the sensitivity of SLIPI and allow smaller deviations in photon trajectory to be detected and thus removed.

5.3. Multiple scattering suppression

To investigate the filtering capabilities of SLIPI in greater detail, the relative amount of light being suppressed is extracted. This is achieved by comparing the conventional results with SLIPI, according to Eq. (8).

$$\varepsilon_{supp} = \frac{I_C - I_S}{I_C} \tag{8}$$

with I_C and I_S representing the intensity curves for conventional imaging and SLIPI presented in Fig. 4 and 5, respectively. The resulting ε_{supp} curves, which are provided in Fig. 8, will thus range between 0 and 1. These values should be interpreted as though either no suppression is performed or all detected light is removed. The small graph provides a magnified part of the curves.

The results in Fig. 8 illustrate how the diffuse light contribution becomes dominant with distance. Close to the entrance, the signal is (in most measurements) characterized by directly scattered light. This can be observed in the conventional intensity curves (Fig. 4), as the influence of signal attenuation is visible here. However, even in this less contaminated region, multiply scattered light dominates when the turbidity is increased. At an optical depth of 6, merely 3 % of the detected light at the entrance contributes to the SLIPI signal when probing 7 μm at S_{32}. Because of the finite dynamic range of the detection system, the signal-to-noise of the SLIPI image is therefore highly reduced when the magnitude of the multiply scattered light greatly exceeds the directly scattered. This upper limitation is seen in the magnified graphs in Fig. 8 (indicated with gray), where the relative suppression becomes constant at $\sim$99.7 %. In these situations, the SLIPI signal is equal to or reduced below the unavoidable camera noise which explains the sudden decrease in both precision and accuracy observed in Table 2 and 3. However, as seen in Fig. 8, this limit is not reached when probing 31 μm because of forward scattering. Based on these and the previous observations it can be concluded that an upper limit, in terms of turbidity, of the SLIPI performance cannot be expressed with a single value but varies depending on the detection system as well as the characteristics of the probed medium.

To expand the range in turbidity over which SLIPI can be implemented a camera system with high dynamic range should be employed. Measurements performed on elastic scattering are often hampered by undesired direct reflection, usually treated by either lowering the amplification on the camera or the laser power to avoid pixel saturation. LIF which normally is "background-free" is therefore beneficial for SLIPI as such light is filtered out prior to detection, thus allowing the dynamic range to be used more efficiently.

#145072 - $15.00 USD Received 30 Mar 2011; revised 12 May 2011; accepted 12 May 2011; published 30 Jun 2011

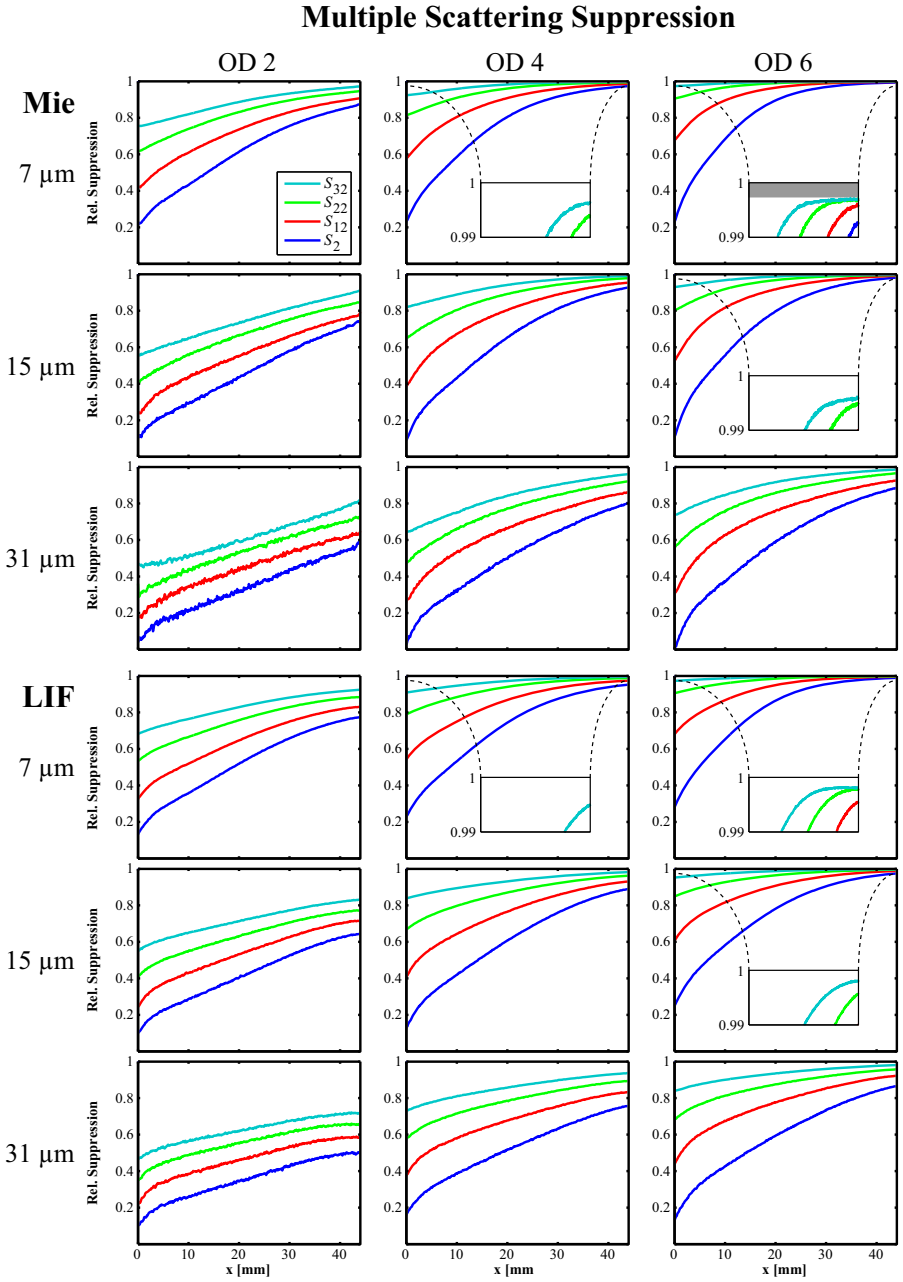

Fig. 8. Relative multiple scattering suppression (ε_{supp}), based on Eq. (8). The small graphs indicate, when needed, a magnified part of the results. The gray area indicates when the suppression becomes constant, at $\varepsilon_{supp} \sim 0.997$.

#145072 - $15.00 USD Received 30 Mar 2011; revised 12 May 2011; accepted 12 May 2011; published 30 Jun 2011

6. Conclusion

The capabilities and limitations of the recently developed imaging technique named SLIPI, capable of suppressing the undesired light contribution arising from multiple scattering events, have been investigated. A homogeneous sample containing a mixture of water and monodisperse polystyrene microspheres doped with dye was probed. The response of the technique with respect to particle size and turbidity was investigated by altering the sample characteristics. It has been demonstrated that by diminishing the diffuse light, SLIPI greatly improves image quality for both Mie scattering and Laser Induced Fluorescence measurements. Furthermore, the SLIPI images present a near exponential reduction of light intensity with distance, tending towards the Beer-Lambert decay.

The results indicate that SLIPI is able to diminish the unwanted contribution of multiply scattered light down to the unavoidable CCD noise level, beyond which no further suppression occurs. This limit, which for the presented measurements is ~ 0.3 %, correlate well with the unavoidable camera noise.

It was further discovered that the diffuse light filtering of SLIPI acts differently depending on the particle size being probed, where measurements performed on smaller particles gives results closer to the Beer-Lambert decay. This is caused by differences in the Mie scattering phase functions, where larger particles have a more pronounced forward scattering lobe (fluorescence also inherent angular scattering characteristics but these are much less pronounced). The filtering processes performed by SLIPI can only suppress photons which deviate from its incident direction. Consequently, multiple scattering events only leading to small changes in photon trajectory cannot be differentiated from directly scattered light. This limitation can be considered as an advantage in terms of visibility because the multiply scattered light that still contain valuable sample information is retained. It is also a disadvantage when a good agreement with the Beer-Lambert law is desired. This becomes important when performing quantitative measurements using SLIPI as this size dependence may influence the accuracy - but not the precision - of the results. Increasing the frequency of the incident modulation could improve the sensitivity of the diffuse light filtering capabilities. Methods of reducing the contribution of multiply scattered light via polarization and spatial filtering for example should also be considered for future developments.

Future work will focus on whether SLIPI can be applied for droplet sizing through the ratio of fluorescence to Mie scattering. This technique, commonly referred to as Planar Droplet Sizing, is based on single scattering detection and has previously been hampered by effects caused by multiple scattering.

Acknowledgment

Finally, the authors wish to show their appreciation to the Linné Center within the Lund Laser Center (LLC) as well as CECOST through SSF and STEM for financial support. Also the ERC Advanced Grant DALDECS is acknowledged.

#145072 - $15.00 USD Received 30 Mar 2011; revised 12 May 2011; accepted 12 May 2011; published 30 Jun 2011